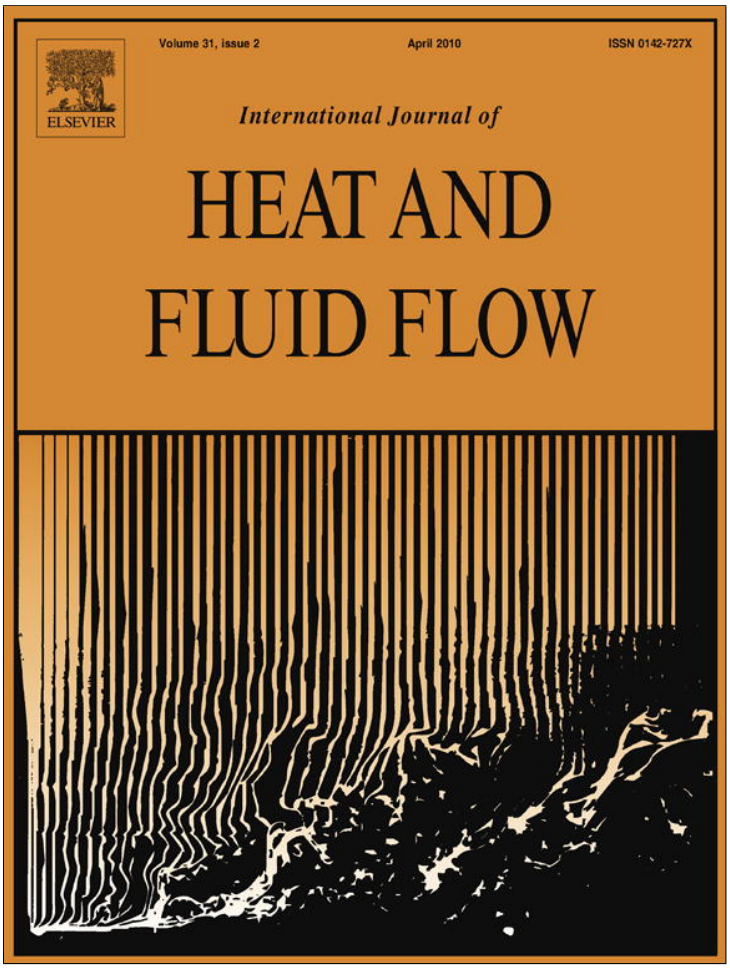
Provided for non-commercial research and education use.
Not for reproduction, distribution or commercial use.



This article appeared in a journal published by Elsevier. The attached copy is furnished to the author for internal non-commercial research and education use, including for instruction at the authors institution and sharing with colleagues.

Other uses, including reproduction and distribution, or selling or licensing copies, or posting to personal, institutional or third party websites are prohibited.

In most cases authors are permitted to post their version of the article (e.g. in Word or Tex form) to their personal website or institutional repository. Authors requiring further information regarding Elsevier's archiving and manuscript policies are encouraged to visit:

http://www.elsevier.com/copyright

Author's personal copy

International Journal of Heat and Fluid Flow 31 (2010) 236–245

Contents lists available at ScienceDirect

International Journal of Heat and Fluid Flow

journal homepage: www.elsevier.com/locate/ijhff

Natural convection heat transfer of nanofluids in a vertical cavity: Effects of non-uniform particle diameter and temperature on thermal conductivity

Kuang C. Lin, Angela Violi *

Department of Mechanical Engineering, University of Michigan, Ann Arbor, MI 48109, USA

ARTICLE INFO

Article history:
Received 2 October 2008
Received in revised form 21 August 2009
Accepted 10 November 2009
Available online 10 February 2010

Keywords:
Non-uniform nanoparticle
Prandtl number
Grashof number
Uncertainties

ABSTRACT

This paper analyzes the heat transfer and fluid flow of natural convection in a cavity filled with Al_2O_3/water nanofluid that operates under differentially heated walls. The Navier–Stokes and energy equations are solved numerically, coupling Xu's model (Xu et al., 2006) for calculating the effective thermal conductivity and Jang's model (Jang et al., 2007) for determining the effective dynamic viscosity, with the slip mechanism in nanofluids. The heat transfer rates are examined for parameters of non-uniform nanoparticle size, mean nanoparticle diameter, nanoparticle volume fraction, Prandtl number, and Grashof number. Enhanced and mitigated heat transfer effects due to the presence of nanoparticles are identified and highlighted. Based on these insights, we determine the impact of fluid temperature on the heat transfer of nanofluids. Decreasing the Prandtl number results in amplifying the effects of nanoparticles due to increased effective thermal diffusivity. The results highlight the range where the heat transfer uncertainties can be affected by the size of the nanoparticles.

© 2009 Elsevier Inc. All rights reserved.

1. Introduction

Heat transfer materials like water, ethylene glycol, engine oil, alumina, copper, and silver have been widely used in numerous important fields, such as heating, ventilating, air-conditioning system, micro-electronics, transportation, manufacturing, and nuclear engineering. Cooling or heating performances for thermal systems play vital roles in the development of energy-efficient heat transfer equipments, such as MEMS and NEMS (Micro and Nano Electro Mechanical Systems, respectively). Over the last years, it has been demonstrated that thermal conductivity of fluids suspended with metallic nanoparticles (nanofluids) is significantly higher than that of pure fluids (Choi, 1995; Choi et al., 2004). Additional benefits of nanofluids include high stability with low sedimentation, no clogging in micro-channels, reduction in pumping power and design of small heat exchanger systems (Murshed et al., 2008).

A great amount of experimental research in this field has recently been reported in literature. Eastman et al. (1997) observed that Al_2O_3/water and CuO/water with 5% nanoparticle volume fractions increased the thermal conductivity by 29% and 60%, respectively. In addition, Xie et al. (2002) showed that Al_2O_3/ethylene glycol with 5% nanoparticle volume fraction enhanced thermal conductivity by 30% and Patel et al. (2003) reported that Au/toluene and Au/water with 0.0013–0.011% nanoparticle volume fractions increased the thermal conductivity by 4–7% and 3.2–5%, respectively.

To explain the observed phenomena, many theoretical studies on the effective thermal conductivity in nanofluids have been proposed over the past few years and the various models can be grouped in two main categories (Murshed et al., 2008). The first one includes a static model for heat conductivity with stationary nanoparticles in multiphase systems, while the second group is based on a dynamic model for heat conductivity. Recently, Xu et al. (2006) derived a new model to describe the heat conduction of nanofluids, based on the fractal distribution of nanoparticles and Brownian motion of nanoparticles for the heat convection between solids and liquids.

On the other hand, research conducted by different groups on heat transfer characteristics of nanofluids has shown little agreement (Murshed et al., 2008). In the natural convection of nanofluids inside a horizontal cylinder, Putra et al. (2003) observed the paradoxical behavior of heat transfer due to different particle concentrations, types of particles and different shapes of the containing cavity. Kim et al. (2004) analyzed the convective instability driven by buoyancy and heat transfer characteristics of nanofluids and indicated that as the thermal conductivity and shape factor of nanoparticles decrease, the convective motion in a nanofluid sets in easily. In a series of experiments in laminar tube flows, Wen and Ding (2004) showed that the local heat transfer coefficients increased 41% and 46% at $Re = 1050$ and 1600, respectively in the presence of nanoparticle volume fraction of 0.016. Jung et al. (2006) reported that the heat transfer coefficient increased 32%

* Corresponding author. Tel.: +1 734 615 6448; fax: +1 734 647 9679.
E-mail address: avioli@umich.edu (A. Violi).

0142-727X/$ - see front matter © 2009 Elsevier Inc. All rights reserved.
doi:10.1016/j.ijheatfluidflow.2009.11.003

Author's personal copy

Nomenclature

c	empirical constant
c_p	specific heat at constant pressure (KJ kg^{-1} K^{-1})
D_f	fractal dimension
d_f	fluid molecular diameter (m)
d_p	mean nanoparticle diameter (m)
Gr	Grashof number $g\beta_f(T_H^* - T_L^*)H^3/\upsilon_f^2$
g	gravitational acceleration (ms^{-2})
H	dimensional cavity height (m)
h	heat convection coefficient (W m^{-2} K^{-1})
k	thermal conductivity of the fluid (W m^{-1} K^{-1})
L	dimensional cavity width (m)
Nu	local Nusselt number
$\overline{Nu}$	average Nusselt number
Pr	Prandtl number, υ_f/α_f
R	ratio of minimum to maximum nanoparticles $d_{p,\min}/d_{p,\max}$
Ra	Rayleigh number $Pr \cdot Gr$
T	dimensionless temperature
t	dimensionless time
u, v	dimensionless velocity components along (x, y) axes
x, y	dimensionless Cartesian coordinates

Greek symbols

α	thermal diffusivity (m^2 s^{-1})
β	thermal expansion coefficient (K^{-1})
ε,η	empirical constant
θ	dependent variables (u, v, p, T, ψ)
ϕ	solid volume fraction
υ_f	kinematic viscosity (m^2 s^{-1})
ω	vorticity (s^{-1})
Ω	dimensionless vorticity, $\omega H^2/\alpha_f$
ψ	dimensionless stream function
ρ	density (kg m^{-3})
μ	dynamic viscosity (kg m^{-1} s^{-1})

Superscripts

$*$	dimensional scale

Subscripts

c	caused by heat convection
eff	effective
f	fluid
H	hot
k	grid point
L	cold
max	maximum
min	minimum
nf	nanofluid
p	nanoparticle
s	solid

by dispersing 1.8% nanoparticles in a micro-rectangular channel with Al_2O_3/water nanofluid. The computational studies reported in this area include two main approaches: (1) a two-phase model, in which both liquid and solid heat transfer behaviors are solved in the flow fields (Wen and Ding, 2005; Mirmasoumi and Behzadmehr, 2008) and (2) a single-phase model, in which solid particles are considered to behave as fluids, because the nanoparticles are easy fluidized (Khanafer et al., 2003; Tiwari and Das, 2007; Abu-Nada, 2008; Akbari et al., 2008; Ho et al., 2008; Abu-Nada and Oztop, 2009). The model of nanofluids in a cavity was first proposed by Khanafer et al. (2003) and the authors investigated the natural convection effect on the enhancement of heat transfer. Tiwari and Das (2007) further studied the forced convection effect with two-sided lid-driven differentially heated square cavity. A theoretical study on a heated cavity reported by Hwang et al. (2007) showed that the heat transfer coefficient of Al_2O_3/water nanofluids is reduced when there is an increase in size of nanoparticles and a decrease in average temperatures. Recently, Ho et al. (2008) adopted four different models for the effective viscosity and thermal conductivity of nanofluids, demonstrating the importance of dynamic viscosity.

In summary, the current computational studies show two limitations: the diameters of the nanoparticles suspended in the fluids are held as uniform and the thermal conductivity models adopted are independent of temperature. In a recent experimental study by Li and Peterson (2007), the authors indicated that the effect of temperature may play an important role in changing the effective thermal conductivity. Prompted by these considerations, in this study we address the effect of non-uniform nanoparticle size and temperature on Al_2O_3/water nanofluid to simulate natural convection in a square cavity. The thermal conductivity and dynamic viscosity of the nanofluid are employed by Xu's model (Xu et al., 2006) and Jang's model (Jang et al., 2007), respectively. The Navier–Stokes and energy equations are coupled with the nanoparticle fractal distributions, mean nanoparticle diameters, nanoparticle volume fraction, Prandtl number, and Grashof number to produce a systematic description of the phenomenon. Therefore, the findings of this study provide more information on the heat transfer characteristics of nanofluids and extend the parameters of previously published enclosure model of Khanafer et al. (2003).

2. Mathematical formulation

Fig. 1 shows the schematic of the model adopted in this study. The origin of the Cartesian coordinate system is at the left corner of the bottom wall located at $y = 0$. The aspect ratio of this enclosure is defined as L/H and assumed to be unity. Initially, the cavity is filled with Al_2O_3/water nanofluid at rest. Fluid motion is then induced by the buoyancy force with the temperature difference between two vertical walls at $x = 0$ and $x = L$. Hot and cold temperatures are kept into the cavity via the vertical walls where nanofluid temperature assumes the prescribed cold temperature $T^* = T_L^*$. The horizontal walls are adiabatic and impermeable to

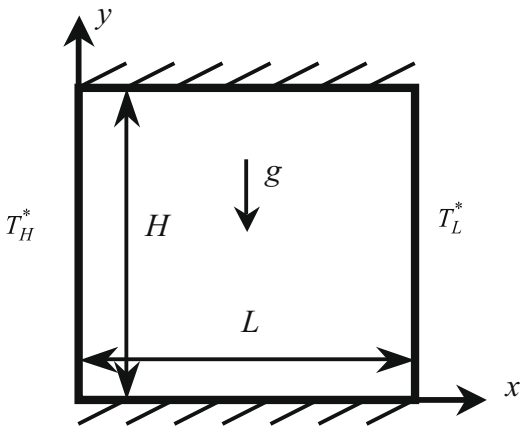


Fig. 1. Schematic of the physical model used in this study.

Author's personal copy

mass transfer. For the velocity field, the no-slip and no penetration assumptions are imposed on the walls.

2.1. Assumptions

The mathematical equations describing the physical model are based on the following assumptions: (I) the thermophysical properties are constant except for the density in the buoyancy force (Boussinesq's hypothesis); (II) the fluid phase and nanoparticles are in a thermal equilibrium state; (III) nanoparticles are spherical; (IV) the nanofluid in the cavity is Newtonian, incompressible, and laminar; and (V) radiation heat transfer between the sides of the cavity is negligible when compared with the other mode of heat transfer.

2.2. Governing equations

The governing equations in dimensional form used in the present study are:

Continuity equation:

$$\frac{\partial u^*}{\partial x^*}+\frac{\partial v^*}{\partial y^*}=0 \tag{1}$$

x-momentum equation:

$$\frac{\partial u^*}{\partial t^*}+u^*\frac{\partial u^*}{\partial x^*}+v^*\frac{\partial u^*}{\partial y^*}=\frac{-1}{\rho_{nf}}\frac{\partial p^*}{\partial x^*}+\frac{\mu_{eff}}{\rho_{nf}}\left(\frac{\partial^2 u^*}{\partial x^{*2}}+\frac{\partial^2 u^*}{\partial y^{*2}}\right) \tag{2}$$

y-momentum equation:

$$\frac{\partial v^*}{\partial t^*}+u^*\frac{\partial v^*}{\partial x^*}+v^*\frac{\partial v^*}{\partial y^*}=\frac{-1}{\rho_{nf}}\frac{\partial p^*}{\partial y^*}+\frac{\mu_{eff}}{\rho_{nf}}\left(\frac{\partial^2 v^*}{\partial x^{*2}}+\frac{\partial^2 v^*}{\partial y^{*2}}\right)+\frac{1}{\rho_{nf}}[(1-\phi)\rho_f\beta_f+\phi\rho_s\beta_s]g(T^*-T_L^*) \tag{3}$$

Energy equation:

$$\frac{\partial T^*}{\partial t^*}+u^*\frac{\partial T^*}{\partial x^*}+v^*\frac{\partial T^*}{\partial y^*}=\alpha_{nf}\left(\frac{\partial^2 T^*}{\partial x^{*2}}+\frac{\partial^2 T^*}{\partial y^{*2}}\right) \tag{4}$$

Vorticity equation and stream function:

$$\omega=\frac{\partial v^*}{\partial x^*}-\frac{\partial u^*}{\partial y^*}=-\left(\frac{\partial^2\psi^*}{\partial x^{*2}}+\frac{\partial^2\psi^*}{\partial y^{*2}}\right) \tag{5}$$

The effective physical properties of the nanofluid in the above equations are:

1. Viscosity:

$$\mu_{eff}=\mu_f(1+2.5\phi)\left[1+\eta\left(\frac{d_p}{H}\right)^{-2\varepsilon}\phi^{2/3}(\varepsilon+1)\right] \tag{6}$$

This well-validated model is presented by Jang et al. (2007) for a fluid containing a dilute suspension of small rigid spherical particles and it accounts for the slip mechanism in nanofluids. The empirical constant ε and η are -0.25 and 280 for Al_2O_3, respectively.

2. Density:

$$\rho_{nf}=(1-\phi)\rho_f+\phi\rho_s \tag{7}$$

3. Heat capacitance:

$$(\rho C_p)_{nf}=(1-\phi)(\rho C_p)_f+\phi(\rho C_p)_s \tag{8}$$

4. Thermal diffusivity:

$$\alpha_{nf}=k_{nf}/(\rho C_p)_{nf} \tag{9}$$

5. Dimensionless stagnant thermal conductivity:

$$\frac{k_{\text{stationary}}}{k_f}=\frac{k_s+2k_f-2\phi(k_f-k_s)}{k_s+2k_f+\phi(k_f-k_s)} \tag{10}$$

This model, introduced by Hamilton and Crosser (H–C model, 1962), considers the nanoparticles in the liquid as stationary.

6. Total dimensionless thermal conductivity of nanofluids:

$$\frac{k_{nf}}{k_f}=\frac{k_{\text{stationary}}}{k_f}+\frac{k_c}{k_f}=\frac{k_s+2k_f-2\phi(k_f-k_s)}{k_s+2k_f+\phi(k_f-k_s)}+c\frac{Nu_p d_f}{Pr}\frac{(2-D_f)D_f}{(1-D_f)^2}\frac{\left[\left(\frac{d_{\max}}{d_{\min}}\right)^{1-D_f}-1\right]^2}{\left(\frac{d_{\max}}{d_{\min}}\right)^{2-D_f}-1}\frac{1}{d_p} \tag{11}$$

This model was proposed by Xu et al. (2006) and it has been chosen in this study to describe the thermal conductivity of nanofluids. The first term is the H–C model and the second term is the thermal conductivity based on heat convection due to Brownian motion. c is an empirical constant, which is relevant to the thermal boundary layer and dependent on different fluids (e.g. $c = 85$ for the deionized water and $c = 280$ for ethylene glycol) but independent of the type of nanoparticles. Nu_p is the Nusselt number for liquid flowing around a spherical particle and equal to two for a single particle in this work. The fluid molecular diameter d_f is taken as 4.5×10^{-10} m for water in present study. The Pr is the Prandtl number, ϕ and d_p are the nanoparticle volume fraction and mean nanoparticle diameter, respectively. The fractal dimension D_f is determined by:

$$D_f=2-\frac{\ln\phi}{\ln(d_{p,\min}/d_{p,\max})} \tag{12}$$

where $d_{p,\max}$ and $d_{p,\min}$ are the maximum and minimum diameters of nanoparticles, respectively. With the given/measured ratio of $d_{p,\min}/d_{p,\max}$, the minimum and maximum diameters of nanoparticles can be obtained with mean nanoparticle diameter d_p from the statistical property of fractal media.

$$d_{p,\max}=d_p\cdot\frac{D_f-1}{D_f}\cdot\left(\frac{d_{p,\min}}{d_{p,\max}}\right)^{-1} \tag{13}$$

$$d_{p,\min}=d_p\cdot\frac{D_f-1}{D_f} \tag{14}$$

By scaling the dimensional variables, the dimensionless form of governing equations can be obtained using the following parameters:

$$x=\frac{x^*}{H},\ y=\frac{y^*}{H},u=\frac{u^*}{\alpha_f/H},\ v=\frac{v^*}{\alpha_f/H},\ t=\frac{\alpha_f t^*}{H^2},$$
$$p=\frac{p^*}{\rho_f(\alpha_f/H)^2},\ T=\frac{T^*-T_L^*}{T_H^*-T_L^*},\ \Omega=\frac{\omega H^2}{\alpha_f},\ \Psi=\frac{\psi^*}{\alpha_f} \tag{15}$$

Variables t, u, v, p, T, Ω, ψ are time, velocity components in x- and y-direction, pressure, temperature, vorticity, and streamline function, respectively.

The 2D dimensionless equations for the conservation of total mass, momentum, and energy of the nanofluid can be written as:

Author's personal copy

Table 1
Comparison of pure fluid solutions with previous works in an enclosure for $Pr = 0.7$ with different Rayleigh numbers.

	Present	Tiwari and Das (2007)	Davis (1983)	Markatos and Pericleous (1984)	Hadjisophocleous et al. (1998)
(a) $Ra = 10^3$					
u_{max}	3.597	3.642	3.649	3.544	3.544
y	0.819	0.804	0.813	0.832	0.814
v_{max}	3.690	3.7026	3.697	3.593	3.586
x	0.181	0.178	0. 178	0.168	0.186
$\overline{Nu}$	1.118	1.0871	1.118	1.108	1.141
(b) $Ra = 10^4$					
u_{max}	16.158	16.1439	16.178	16.18	15.995
y	0.819	0.822	0.823	0.832	0.814
v_{max}	19.648	19.665	19.617	19.44	18.894
x	0.112	0.110	0.119	0.113	0.103
$\overline{Nu}$	2.243	2.195	2.243	2.201	2.29
(c) $Ra = 10^5$					
u_{max}	36.732	34.30	34.73	35.73	37.144
y	0.858	0.856	0.855	0.857	0.855
v_{max}	68.288	68.7646	68.59	69.08	68.91
x	0.063	0.05935	0.066	0.067	0.061
$\overline{Nu}$	4.511	4.450	4.519	4.430	4.964
(d) $Ra = 10^6$					
u_{max}	66.46987	65.5866	64.63	68.81	66.42
y	0.86851	0.839	0.85	0.872	0.897
v_{max}	222.33950	219.7361	217.36	221.8	226.4
x	0.03804	0.04237	0.0379	0.0375	0.0206
$\overline{Nu}$	8.757933	8.803	8.799	8.754	10.39

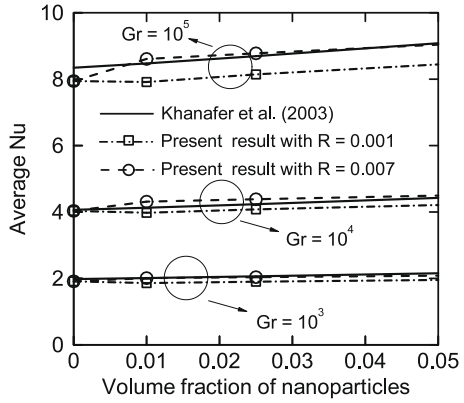


Fig. 2. Comparison of average Nusselt numbers between Khanafer et al. (2003) and the present result for $Pr = 6.2$ and $d_p = 10$ nm with $Gr = 10^3$, $Gr = 10^4$, and $Gr = 10^5$.

Continuity equation:

$$\frac{\partial u}{\partial x} + \frac{\partial v}{\partial y} = 0 \tag{16}$$

x-momentum equation:

$$\frac{\partial u}{\partial t} + u\frac{\partial u}{\partial x} + v\frac{\partial u}{\partial y} = \frac{-\rho_f}{\rho_{nf}}\frac{\partial p}{\partial x} + \frac{\mu_{eff}Pr}{\rho_{nf}\nu_f}\left(\frac{\partial^2 u}{\partial x^2} + \frac{\partial^2 u}{\partial y^2}\right) \tag{17}$$

y-momentum equation:

$$\frac{\partial v}{\partial t} + u\frac{\partial v}{\partial x} + v\frac{\partial v}{\partial y} = \frac{-\rho_f}{\rho_{nf}}\frac{\partial p}{\partial y} + \frac{\mu_{eff}Pr}{\rho_{nf}\nu_f}\left(\frac{\partial^2 v}{\partial x^2} + \frac{\partial^2 v}{\partial y^2}\right) + \frac{(1-\phi)\rho_f\beta_f + \phi\rho_s\beta_s}{\rho_{nf}\beta_f}Pr^2GrT \tag{18}$$

where $Gr = g\beta_f(T_H^* - T_L^*)H^3/\upsilon_f^2$ is the Grashof number and defined as the ratio of the buoyancy to viscous force.

Energy equation:

$$\frac{\partial T}{\partial t} + u\frac{\partial T}{\partial x} + v\frac{\partial T}{\partial y} = \frac{\alpha_{nf}}{\alpha_f}\left(\frac{\partial^2 T}{\partial x^2} + \frac{\partial^2 T}{\partial y^2}\right) \tag{19}$$

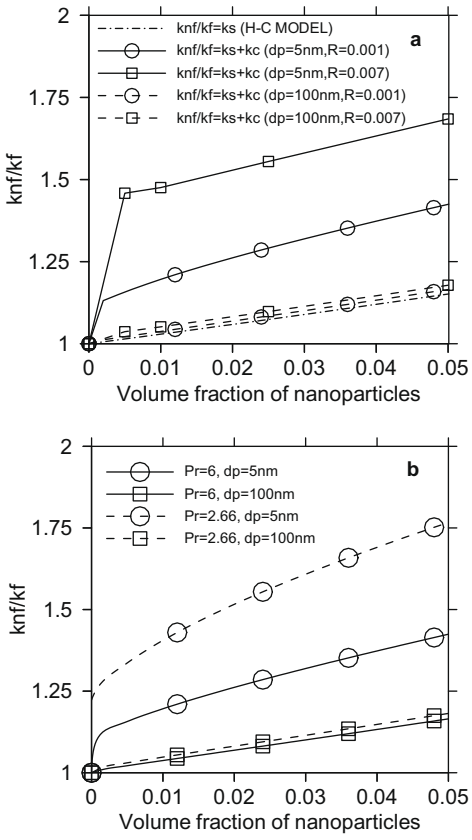


Fig. 3. Dimensionless effective thermal conductivity of Al_2O_3/water nanofluid versus concentration ϕ of nanoparticles with different mean nanoparticle diameters and fractal distributions: (a) $Pr = 6$ and (b) $R = 0.001$.

Vorticity equation and stream function:

$$\Omega = \frac{\partial v}{\partial x} - \frac{\partial u}{\partial y} = -\left(\frac{\partial^2 \Psi}{\partial x^2} + \frac{\partial^2 \Psi}{\partial y^2}\right) \tag{20}$$

Author's personal copy

The initial conditions are

$$u = v = T = \psi = 0 \quad \text{at} \quad t = 0 \tag{21}$$

and the boundary conditions applied at $t > 0$ can be summarized as follows:

$$\begin{aligned} &u = v = \psi = \frac{\partial T}{\partial y} = 0; \quad \text{at} \quad y = 0 \quad \text{and} \quad 1 \text{ for } \quad 0 < x < 1, \\ &T = 1, u = v = \psi = 0; \quad \text{at} \quad x = 0 \quad \text{for } 0 \leqslant y \leqslant 1, \\ &T = 0, u = v = \psi = 0; \quad \text{at} \quad x = 1 \quad \text{for } 0 \leqslant y \leqslant 1 \end{aligned} \tag{22}$$

2.3. Nusselt number

The Nusselt number, *Nu*, is expected to depend on a number of factors such as thermal conductivity, heat capacitance, viscosity, flow structure of nanofluids, volume fraction, dimensions, and fractal distributions of nanoparticles. The local variation of the Nusselt number of the fluid can be expressed as:

$$Nu = -\frac{k_{nf}}{k_f}\frac{\partial T}{\partial x} \tag{23}$$

By integrating the local Nusselt number over the left wall, the average Nusselt number along the left wall is given as:

$$\overline{Nu} = \int_0^1 Nu dy \tag{24}$$

3. Numerical method

Eqs. (16)–(20) are discretized on a structured grid. The velocity components (u, v) and the scalar variables (pressure, temperature, vorticity, and streamline function) are located at the center of the control volume in a non-staggered manner. The governing equations are solved numerically by a weighting function scheme (Lee, 1989a). The Non-Staggered Artificial Pressure for Pressure-Linked Equation (NAPPLE) algorithm (Lee and Tzong, 1992) is used to convert the continuity Eq. (16) into a pressure-linked equation. Compared with other algorithms of staggered grid systems, this method has the advantage of high computational efficiency and simple grid structure. The solutions of discretized equations are obtained using a Semi-Implicit Solver (SIS; Lee, 1989b) and iterated till convergence. θ_{new} are the new solutions obtained from the SIS iteration and $\theta_{\max}$ and $\theta_{\min}$ are the maximum and minimum values of θ_{new}. The prescribed tolerance TOL = 10^{-6} is:

$$\underset{k=1\ldots m}{Max}\left|\frac{\theta_{k,new} - \theta_{k,old}}{\theta_{\max} - \theta_{\min}}\right| \leqslant \text{TOL} \tag{25}$$

where m is the last point in the computational domain. For a better convergence rate, the guess solution θ_k is modified by employing a successive over-relaxation (SOR) factor:

$$\theta_{k+1} = \theta_k + \text{SOR}(\theta_{k+1} - \theta_k) \tag{26}$$

At each time step, the converged solution is used as the initial condition for the following time step. The method employed to solve the time differential terms is an unconditionally stable fully implicit scheme.

Table 2
Thermophysical properties of different phases.

Properties	Fluid phase (water, 300 K)	Fluid phase (water, 340 K)	Solid phase (Al_2O_3)
c_p (J/kg K)	4179	4188	850
ρ (kg/m^3)	997.1	879.4	3900
k (W/m K)	0.61	0.66	46
β (K^{-1})	2.1×10^{-4}	5.66×10^{-4}	1.67×10^{-5}

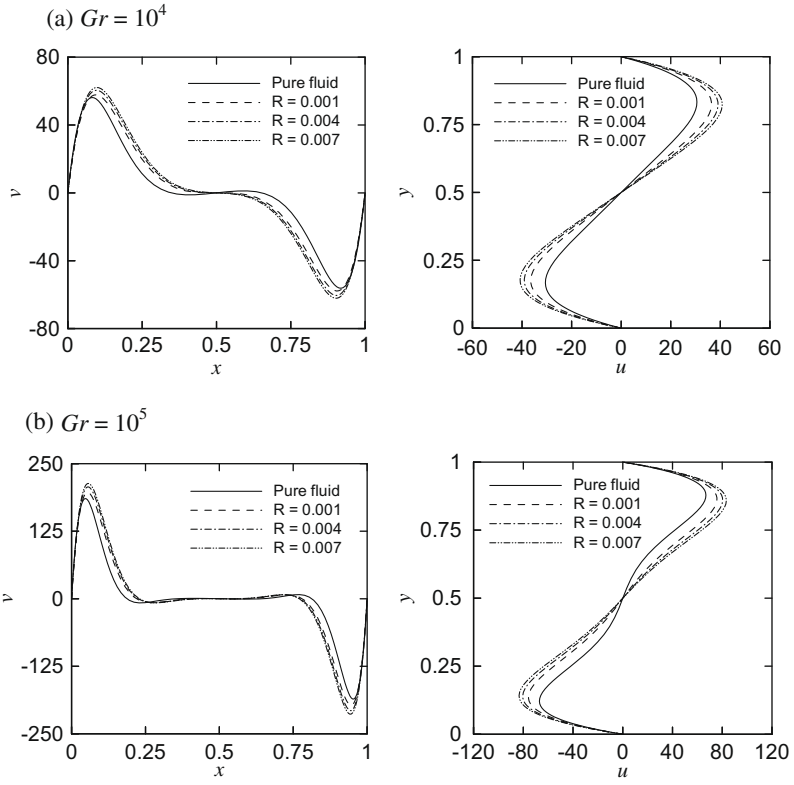


Fig. 4. Velocity profiles at enclosure centerline for different values of $R = d_{p,\min}/d_{p,\max}$ with $Pr = 6$, $d_p = 5$ nm, and $\phi = 0.05$.

Author's personal copy

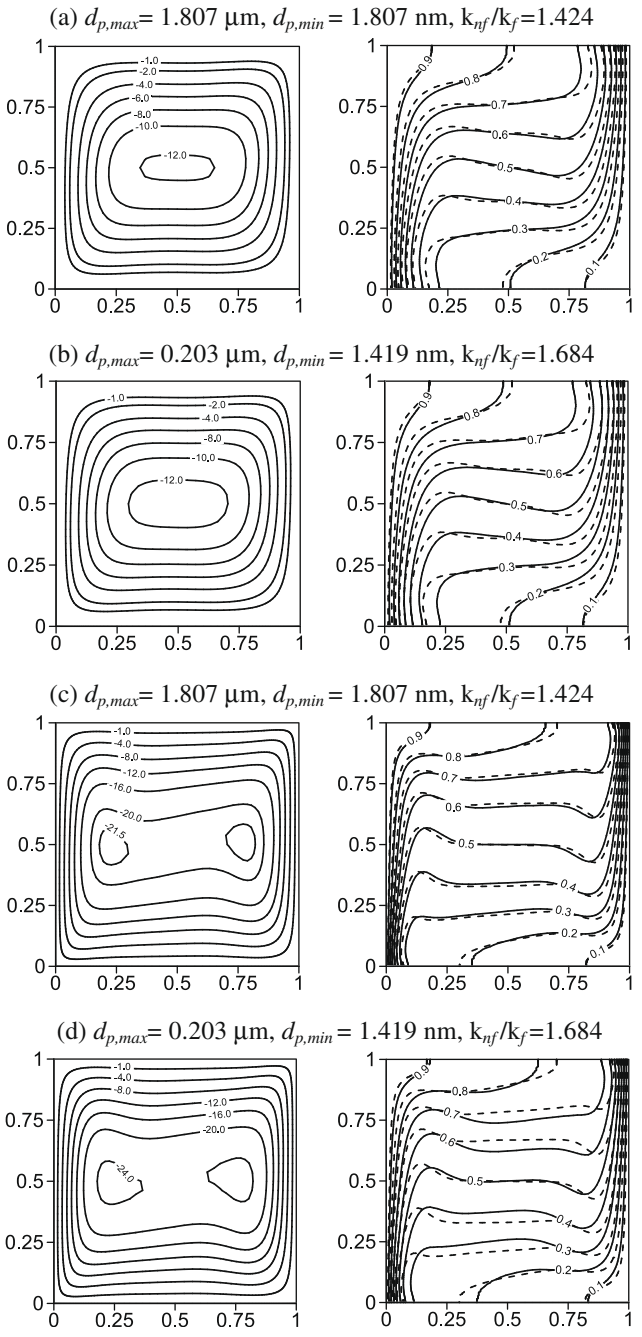


Fig. 5. Streamlines and comparison of isotherm contours between nanofluids (–) and pure fluid (- - -) with different values of: (a) $R = 0.001$, $Gr = 10^4$; (b) $R = 0.007$, $Gr = 10^4$; (c) $R = 0.001$, $Gr = 10^5$; and (d) $R = 0.007$, $Gr = 10^5$ for $Pr = 6$, $d_p = 5$ nm, and $\phi = 0.05$.

4. Algorithm validation

The validity of the numerical approach has been assessed by grid-independence and by comparisons with the results in the literature on steady 2D square cavity flows of buoyancy-driven laminar heat transfer. To capture the rapid changes in the dependent variables, in this study we implement the non-uniform grid system with more nodes accumulated near the walls. Different non-uniform grids of 41×41, 81×81, 121×121, and 161×161 are examined for $Gr = 10^5$, $Pr = 6$, $\phi = 0.05$, $d_p = 5$ nm, and $R = 0.001$ and we observe that the further refinement from 121×121 grid is not necessary. The average Nusselt number is 9.45, 9.51, 9.52, and 9.52 for 41×41, 81×81, 121×121, and 161×161 points, respectively. Therefore, a 121×121 grid is chosen to calculate the flow and heat transfer behavior over the range of operational parameter values considered.

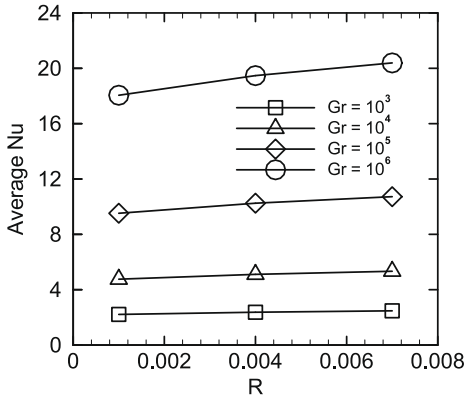


Fig. 6. Variation of average *Nu* numbers with the ratio $R = d_{p,\min}/d_{p,\max}$ for constant values of *Gr* numbers with $Pr = 6$, $d_p = 5$ nm, and $\phi = 0.05$.

To ensure the accuracy and validity of the new model, we analyze a system composed of pure fluid in an enclosure with $Pr = 0.7$ and different *Ra* numbers. This system has been studied by other research groups, including Tiwari and Das (2007), Davis (1983), Markatos and Pericleous (1984), and Hadjisophocleous et al. (1998). Table 1 shows the comparison between the results obtained with the new model and the values presented in the literature. The quantitative comparisons for the average Nusselt numbers along the hot wall and the maximum velocity values and their corresponding locations indicate an excellent agreement. In addition, we investigate a differentially heated square enclosure with different volume fractions of nanoparticles and compared the average *Nu* numbers obtained with the new model with the results reported in the literature by Khanafer et al. (2003). As shown in Fig. 2, the new model is able to reproduce the previous results and the effect of non-uniform nanoparticle size.

In order to evaluate Xu's model, Fig. 3 shows the characteristic of the effective thermal conductivity, which is a function of the practical parameters $R = d_{p,\min}/d_{p,\max}$, d_p and Prandtl number. *R* has relatively high effect for small mean nanoparticle diameters as reported in Fig. 3a. The temperature effect of nanofluids is described in terms of the Prandtl number. In Fig. 3b, the Prandtl numbers are 6 and 2.66 for temperature of 300 and 340 K, respectively and consequently the presence of nanoparticles has the strong effect on heat conductivity of the nanofluid at high temperatures. Thus, compared with the traditional H–C model with the assumption of uniform nanoparticle size, Xu's model shows a better flexibility in predicting the heat transfer characteristic.

5. Results and discussion

The overall objective of this current investigation is to explore the heat transfer behavior of natural convection inside a cavity with Al_2O_3/water nanofluid. Specifically, we will analyze steady-state flow fields, temperature fields, and heat transfer rates for various values of the Grashof number, Prandtl number, ratio of minimum to maximum nanoparticle diameter, mean nanoparticle diameter, and nanoparticle volume fraction. As reported in various studies (Khanafer et al., 2003; Xu et al., 2006; Jang et al., 2007; Tiwari and Das, 2007; Abu-Nada, 2008; Akbari et al., 2008; Abu-Nada and Oztop, 2009), the ranges of variation of these parameters are $10^3 \leqslant Gr \leqslant 10^6$, $2.66 \leqslant Pr \leqslant 6$, $0.001 \leqslant R \leqslant 0.007$,

Author's personal copy

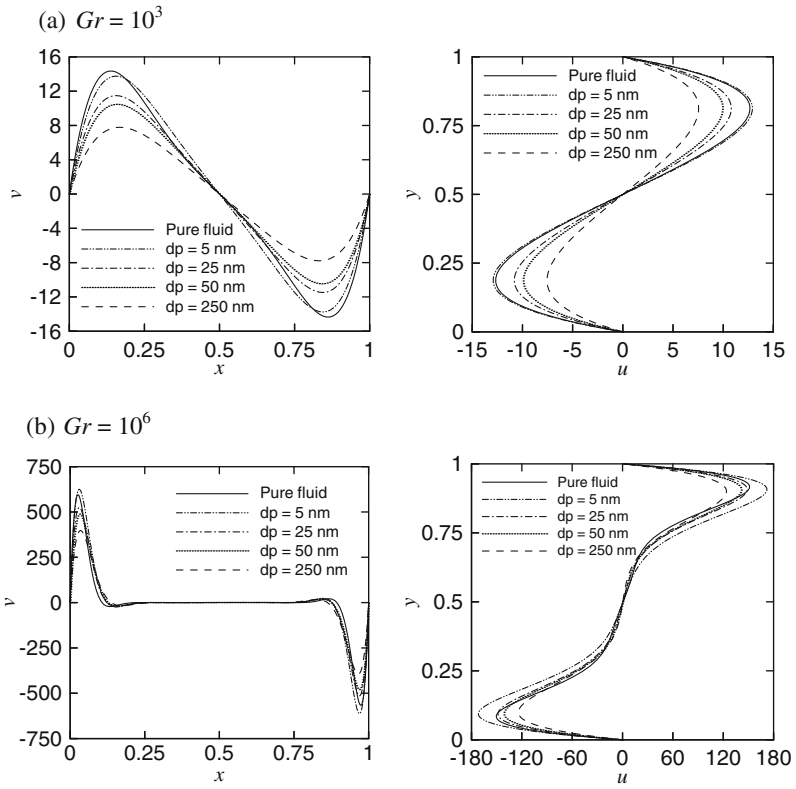


Fig. 7. Velocity profiles at enclosure centerline for different values of d_p with $Pr = 6$, $R = 0.001$, and $\phi = 0.05$.

5 nm $\leqslant d_p \leqslant$ 250 nm, and $0 \leqslant \phi \leqslant 0.05$. Table 2 shows the thermophysical properties of fluid and solid phases.

The results below are organized as follows. In Sections 5.1 and 5.2, we report on effects of non-uniform nanoparticle diameter and mean nanoparticle diameter, respectively on the heat transfer. The effect of temperature on the nanofluid heat transfer is discussed in Section 5.3 and finally the characteristics of the heat transfer as function of the nanoparticle volume fraction are analyzed in Section 5.4.

5.1. Effect of non-uniform nanoparticle diameter

The effect of fractal distributions on the heat transfer is reported below in terms of the ratio of minimum to maximum nanoparticle diameter R, while the mean diameter and nanoparticle volume fraction and the Prandtl number are fixed at 5 nm, 5%, and 6%, respectively. It is worth mentioning that from Eq. (12), the fractal dimension D_f, derived from Brownian motion in the nanofluid, is inversely proportional to $R = d_{p,\min}/d_{p,\max}$ and this implies that R values provide a measure of the importance of the non-uniform nanoparticle structures. The steady-state variation of the velocity in the mid-section of the cavity is analyzed for $Gr = 10^4$ and $Gr = 10^5$. Fig. 4 shows that the heat convection of the nanofluid increases remarkably with R due to an increase in the energy transport through the fluid. The phenomenon can be explained based on the Brownian motion theory that relates small particles to high velocity.

Fig. 5 illustrates the effect of R on the steady-state variation of the streamlines and isotherms for $Gr = 10^4$ and $Gr = 10^5$. The intensity of flow activities is documented by recording the values of streamline contours. In this physical model, the flow patterns are characterized by a primary recirculating clockwise vortex that occupies the bulk of the cavity. As R increases from 0.001 to 0.007, the flow patterns remain quite the same while the absolute circulation strength is enhanced due to relatively high velocity of the fluid flow. To explain this phenomenon, we determine the maximum and minimum diameters from Eqs. (13) and (14). It is interesting to note that for a fixed mean nanoparticle diameter, the maximum and minimum diameters of nanoparticles are both decreased by relatively high R values (Fig. 5). This analysis basically implies that at a constant volume fraction, the heat convection is better enhanced by relatively small nanoparticles with more uniform size. Therefore, with these nanoparticle structures, the value of dimensionless thermal conductivity k_{nf}/k_f increases by 18.26% from $R = 0.001$ to 0.007. The comparisons of the pure fluid and nanofluid isotherms show that vertical stratification of the isotherms breaks down with an increase in R at relatively high Grashof numbers. This behavior can be attributed to the increase of thermal conductivity and gravity.

The average Nusselt number for these conditions is calculated using Eq. (24) and the result reported in Fig. 6 shows that the higher the Gr number, the larger the heat transfer. Over the range of R values studied, the average Nusselt number increases 7.9% and 12.94% for $Gr = 10^3$ and $Gr = 10^6$, respectively. As a consequence, nanofluids enhance heat transfer in both large and small buoyancy conditions.

5.2. Effect of mean nanoparticle diameter

To study the effect of the mean nanoparticle diameter on the heat transfer, we vary the diameter between 5 nm and 250 nm, while R, Pr, and ϕ are fixed at 0.001, 6, and 0.05, respectively. The results of velocity profiles are shown in Fig. 7. As the mean nanoparticle diameter increases, the corresponding flow velocity decreases and hence the heat transfer enhancement is reduced. Notice that the fluids suspended with Al_2O_3 nanoparticles mitigate the fluid flow in the cavity except for $d_p = 5$ nm when compared with the pure fluid. This phenomenon is mainly caused by the

Author's personal copy

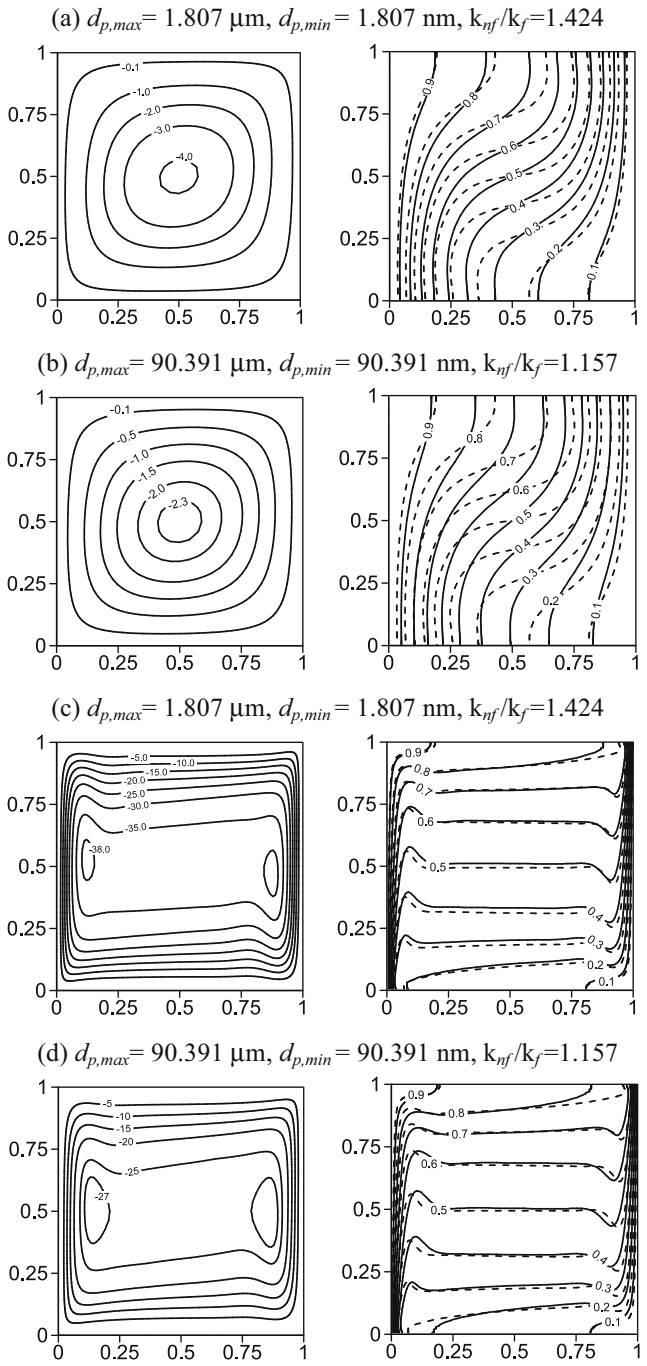


Fig. 8. Streamlines and comparison of isotherm contours between nanofluids (—) and pure fluid (- - -) with different values of: (a) d_p = 5 nm, $Gr = 10^3$; (b) d_p = 250 nm, $Gr = 10^3$; (c) d_p = 5 nm, $Gr = 10^6$; and (d) d_p = 250 nm, $Gr = 10^6$ for Pr = 6, R = 0.001, and ϕ = 0.05.

effective dynamic viscosity, which dominates the heat transfer characteristic of nanofluid flow as the k_{nf}/k_f reaches unity.

Fig. 8 shows the streamline and temperature contours for d_p = 5 and 250 nm with $Gr = 10^3$ and 10^6. Similarly to the results reported in Fig. 5, the streamline patterns are not significantly affected by the mean nanoparticle diameters. However, the value of absolute circulation strength decreases with an increase in the mean nanoparticle diameter. The effective thermal conductivity increases by 23.8% as the mean nanoparticle diameter is reduced from 250 to 5 nm. Consequently, decreasing the diameters of nanoparticles has qualitatively the same effect increasing R.

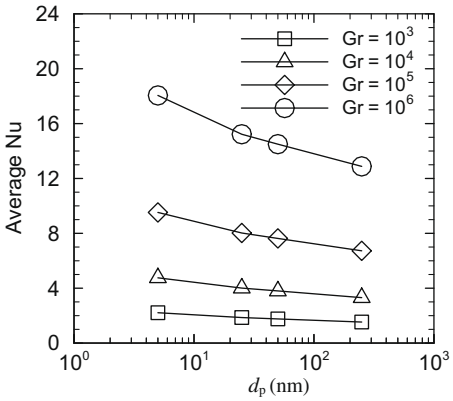


Fig. 9. Variation of average Nu numbers with the mean nanoparticle diameters for constant values of Gr numbers with Pr = 6, R = 0.001, and ϕ = 0.05.

Fig. 9 shows the average Nusselt number computed with different mean nanoparticle diameters for various Grashof numbers. It is evident that the average Nusselt number varies significantly with the mean nanoparticle diameter between 5 and 50 nm. By decreasing the mean diameters of nanoparticles from 250 to 5 nm, the

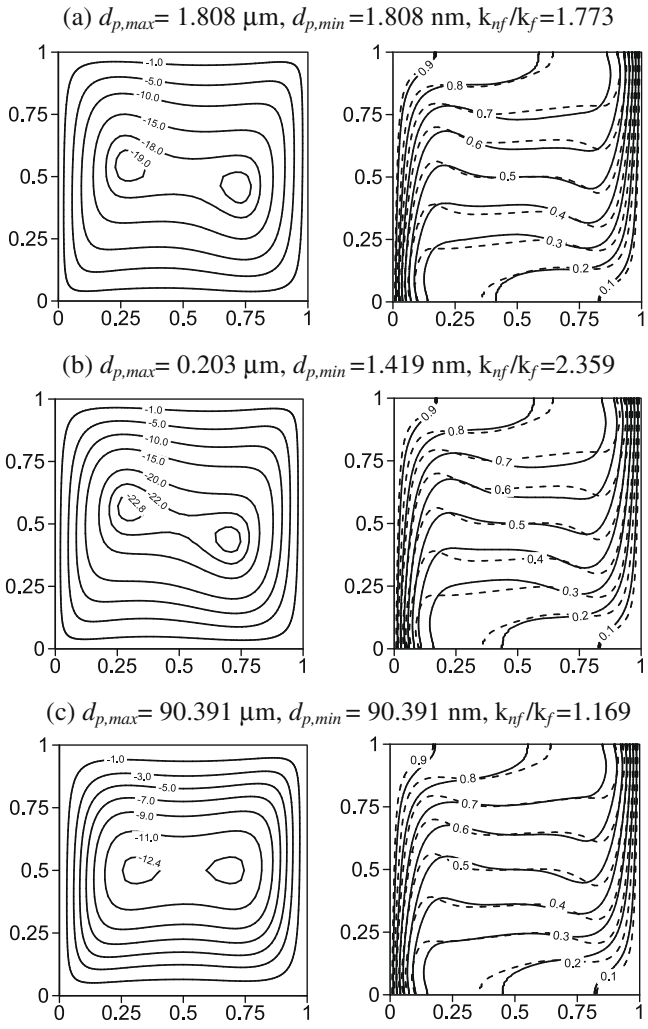


Fig. 10. Streamlines and comparison of isotherm contours between nanofluids (—) and pure fluid (- - -) with different values of: (a) R = 0.001, d_p = 5 nm; (b) R = 0.007, d_p = 5 nm; (c) R = 0.001, d_p = 250 nm for Pr = 2.66, $Gr = 10^5$ and ϕ = 0.05.

Author's personal copy

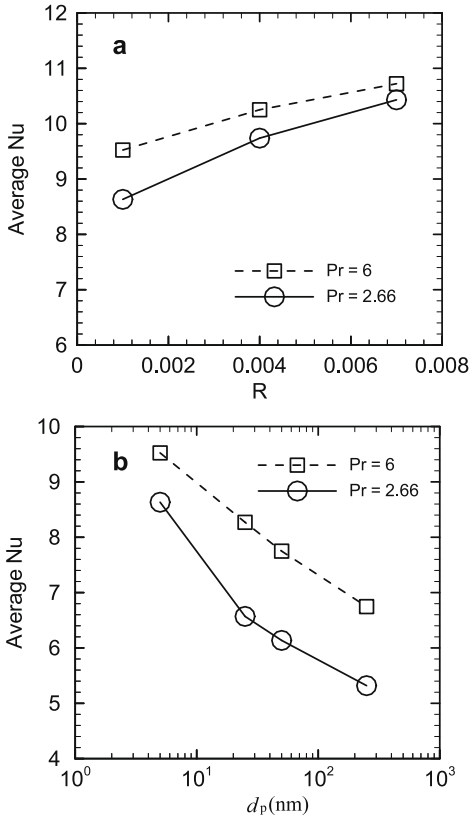


Fig. 11. (a) Variation of average *Nu* number with the ratio $R = d_{p,\min}/d_{p,\max}$ at $Gr = 10^5$, $d_p = 5$ nm, and $\phi = 0.05$ and for different values of *Pr* numbers. (b) Variation of average *Nu* numbers with the mean nanoparticle diameters at $Gr = 10^5$, $R = 0.001$, and $\phi = 0.05$ and for different values of *Pr* numbers.

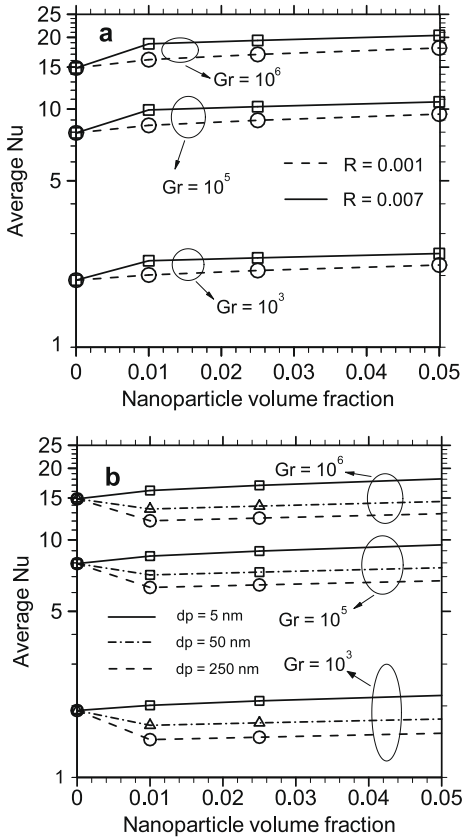


Fig. 12. Variation of average *Nu* numbers with ϕ for: (a) different values of *R* and *Gr* numbers at $Pr = 6$ and $d_p = 5$ nm and (b) different values of d_p and *Gr* numbers at $Pr = 6$ and $R = 0.001$.

heat transfer with different Grashof numbers increases 44.3% and 40.15% for $Gr = 10^3$ and $Gr = 10^6$, respectively.

5.3. Effect of nanofluid temperature

In the previous section, we determine that the physical properties of nanoparticles have a significant effect on the heat transfer of natural convection, as the diameter of nanoparticles is decreased. There is interplay between momentum equations and effective thermal conductivity as the nanofluid temperature is increased. For natural convection, it is known that the Nusselt number is proportional to the Prandtl number for pure fluids. However, Eq. (11) reveals that the effective thermal conductivity is inversely proportional to the Prandtl number and hence, the heat transfer characteristics of nanofluids as function of temperature are not immediately clear.

In this section, the effect of temperature on the heat transfer is studied considering $Gr = 10^5$ and varying *R* and d_p at $Pr = 2.66$ and $\phi = 0.05$. The effects of *R* on the predicted streamlines and isotherms are displayed in Fig. 10a and b for $Pr = 2.66$ and $d_p = 5$ nm. As *R* changes from 0.001 to 0.007, the flow patterns with two prime vortices are similar and the isotherm contours illustrate the significant variations due to the low Prandtl number. Compared with the results reported in Fig. 5c and d, the effect of *R* is more important at relatively high temperatures. Similarly, Fig. 10a and c demonstrate that the effect of mean nanoparticle diameter significantly influences streamlines and isotherms.

Fig. 11a shows the average Nusselt number as a function of *R* for different Prandtl numbers. The results clearly indicate that the heat transfer enhancement at $Pr = 2.66$ is approximately 40% more effective than that at $Pr = 6$. Similarly, Fig. 11b presents the average Nusselt number as a function of d_p for different Prandtl numbers. It is evident that heat transfer enhancement at $Pr = 2.66$ is 50% stronger than that at $Pr = 6$.

5.4. Effect of nanoparticle volume fraction

In this last section we analyze the effect of the nanoparticle volume fraction ϕ (from 0 to 0.05) on the heat transfer characteristics. Fig. 12a and b report the effect of the *R* and d_p, respectively on the average *Nu* number. For both cases, the Grashof numbers are varied from 10^3 to 10^6, while the *Pr* is fixed at six. In Fig. 12a the effect of *R* versus the average Nusselt number is plotted for $d_p = 5$ nm. The results indicate that as *R* changes from 0.001 to 0.007, the average Nusselt number rapidly increases for different Grashof numbers. Similarly, Fig. 12b presents the average Nusselt number versus ϕ with various mean nanoparticle diameters. As d_p is increased to 50 nm, the average Nusselt number of nanofluids becomes lower than that of pure fluids for different Grashof numbers. This mitigation of heat transfer is mainly attributed to the effective dynamic viscosity, which is predominant in the natural convection of nanofluids for low effective thermal conductivity. Overall, the analysis also defines the operating range where Al_2O_3/water nanofluid can be considered effectively in determining the level of heat transfer augmentation.

6. Conclusions

The current investigation is concerned with heat and fluid flow of natural convection in a cavity filled with Al_2O_3/water nanofluid

Author's personal copy

that operates under differentially heated walls. The results of this work illustrate that the heat transfer characteristics of the nanofluid can be enhanced as the ratio of minimum to maximum nanoparticle diameter is increased from 0.001 to 0.007 or the mean nanoparticle diameter is decreased from 250 to 5 nm. These phenomena can be attributed to the dominant effect of the Brownian motion caused by heat convection. However, the heat transfer performance of the nanofluid compared with the pure fluids becomes less significant as the dimensionless total thermal conductivity of the nanofluid is close to unity due to the increase of nanoparticle sizes. This contradictory effect of nanofluids is mainly caused by the effective dynamic viscosity.

The increase of nanofluid temperature is found to augment both the effects of non-uniform nanoparticle diameter and mean nanoparticle diameter inside the cavity. For small and large Grashof numbers, the systems behave similarly in terms of heat transfer enhancement because the heat conduction is dominated by high thermal conductivity of nanofluids.

The results for the effect of nanoparticle volume fraction establish the range of operating nanoparticle parameters where transport activities can be manipulated. Future work is recommended to extend the current investigation to a model with concentration distributions of nanoparticles. This model shall aid in examining the contribution of the effect of particle migration in augmenting the heat transfer in the present configuration.

References

Abu-Nada, E., 2008. Application of nanofluids for heat transfer enhancement of separated flows encountered in a backward facing step. Int. J. Heat Fluid Flow 29, 242–249.

Abu-Nada, E., Oztop, H.F., 2009. Effects of inclination angle on natural convection in enclosures filled with Cu–water nanofluid. Int. J. Heat Fluid Flow 30, 669–678.

Akbari, M., Behzadmehr, A., Shahraki, F., 2008. Fully developed mixed convection in horizontal and inclined tubes with uniform heat flux using nanofluids. Int. J. Heat Fluid Flow 29, 545–556.

Choi, S.U.S., 1995. Enhancing thermal conductivity of fluids with nanoparticles. In: Siginer, D.A., Wang, H.P. (Eds.), Developments and Applications of Non-Newtonian Flows, vol. FED-231/MD-66. ASME, Berlin, pp. 99–105.

Choi, S.U.S., Zhang, Z.G., Keblinski, P., 2004. Nanofluids. Encyclopedia of Nanoscience and Nanotechnology 6, 757–773.

Davis, G.D.V., 1983. Natural convection of air in a square cavity: a benchmark solution. Int. J. Numer. Meth. Fluids 3, 249–264.

Eastman, J.A., Choi, S.U.S., Li, S., Thompson, L.J., 1997. Enhanced thermal conductivity through the development of nanofluids. Proceeding of the Symposium on Nanophase and Nanocomposite Materials II, vol. 457. Materials Research Society, USA, pp. 3–11.

Hadjisophocleous, G.V., Sousa, A.C.M., Venart, J.E.S., 1998. Predicting the transient natural convection in enclosures of arbitrary geometry using a nonorthogonal numerical model. Numer. Heat Transfer A 13, 373–392.

Hamilton, R.L., Crosser, O.K., 1962. Thermal conductivity of heterogeneous two component systems. Indus. Eng. Chem. Fund. 1, 187–191.

Ho, C.J., Chen, M.W., Li, Z.W., 2008. Numerical simulation of natural convection of nanofluid in a square enclosure: effects due to uncertainties of viscosity and thermal conductivity. Int. J. Heat Mass Transfer 51, 4506–4516.

Hwang, K.S., Lee, J.H., Jang, S.P., 2007. Buoyancy-driven heat transfer of water-based Al_2O_3 nanofluids in a rectangular cavity. Int. J. Heat Mass Transfer 50, 4003–4010.

Jang, S.P., Lee, J.H., Hwang, K.S., Choi, S.U.S., 2007. Particle concentration and tube size dependence of viscosities of Al_2O_3-water nanofluids flowing through micro- and minitubes. Appl. Phys. Lett. 91, 243112.

Jung, J.Y., Oh, H.S., Kwak, H.Y., 2006. Forced convective heat transfer of nanofluids in microchannels. In: Proceedings of ASME Int. Mech. Eng. Congress and Exposition (IMECE 2006), Chicago, USA.

Khanafer, K., Vafai, K., Lightstone, M., 2003. Buoyancy-driven heat transfer enhancement in a two-dimensional enclosure utilizing nanofluids. Int. J. Heat Mass Transfer 46, 3639–3653.

Kim, J., Kang, Y.T., Choi, C.K., 2004. Analysis of convective instability and heat transfer characteristics of nanofluids. Physics of Fluids 16, 2395–2401.

Lee, S.L., 1989a. Weighting function scheme and its application on multidimensional conservation equations. Int. J. Heat Mass Transfer 32, 2065–2073.

Lee, S.L., 1989b. A strongly implicit solver for two-dimensional elliptic differential equations. Numer. Heat Transfer B 16, 161–178.

Lee, S.L., Tzong, R.Y., 1992. Artificial pressure for pressure-linked equation. Int. J. Heat Mass Transfer 35, 2705–2716.

Li, C.H., Peterson, G.P., 2007. Experimental investigation of temperature and volume fraction variations on the effective thermal conductivity of nanoparticle suspensions. J. Appl. Phys. 99, 084314-1–084314-8.

Markatos, N.C., Pericleous, K.A., 1984. Laminar and turbulent natural convection in an enclosed cavity. Int. J. Heat Mass Transfer 27, 755–772.

Mirmasoumi, S., Behzadmehr, A., 2008. Effect of nanoparticles mean diameter on mixed convection heat transfer of a nanofluids in a horizontal tube. Int. J. Heat Fluid Flow 29, 557–566.

Murshed, S.M.S., Leong, K.C., Yang, C., 2008. Thermophysical and electrokinetic properties of nanofluids – A critical review. Appl. Therm. Eng. 28, 2109–2125.

Patel, H.E., Das, S.K., Sundararajan, T., Nair, A.S., George, B., Pradeep, T., 2003. Thermal conductivity of naked and monolayer protected metal nanoparticles based nanofluids: manifestation of anomalous enhancement and chemical effects. Appl. Phys. Lett. 83, 2931–2933.

Putra, N., Roetzel, W., Das, S.K., 2003. Natural convection of nano-fluids. Heat Mass Transfer 39, 775–784.

Tiwari, R.K., Das, M.K., 2007. Heat transfer augmentation in a two-sided lid-driven differentially heated square cavity utilizing nanofluids. Int. J. Heat Mass Transfer 50, 2002–2018.

Wen, D., Ding, Y., 2004. Convective heat transfer of nanofluids at the entrance region under laminar flow conditions. Int. J. Heat Mass Transfer 47, 5158–5188.

Wen, D., Ding, Y., 2005. Effect of particle migration on heat in suspensions of nanoparticles flowing through minichannels. Microfluid. Nanofluid. 1, 183–189.

Xie, H., Wang, J., Xi, T., Liu, Y., Ai, F., Wu, Q., 2002. Thermal conductivity enhancement of suspensions containing nanosized alumina particles. J. Appl. Phys. 91, 4568–4572.

Xu, J., Yu, B., Zou, M., Xu, P., 2006. A new model for heat conduction of nanofluids based on fractal distributions of nanoparticles. J. Phys. D 39, 4486–4490.